J Mater Sci (2017) 52:218–228

Plasmon-enhanced optical absorption with graded bandgap in diamond-like carbon (DLC) films

B. Ghosh[1,*], F. Guzmán-Olivos[2], and R. Espinoza-González[1]

[1] LAM, Material Science Department, FCFM, U. de Chile, Santiago, Chile
[2] Laboratory of Surfaces, Physics Department, FCFM, U. de Chile, Santiago, Chile

Received: 29 May 2016
Accepted: 20 August 2016
Published online: 30 August 2016

ABSTRACT

Diamond-like carbon (DLC) films with tunable optical bandgap (E_g) were successfully deposited on glass and n-Si (100) substrates by radio frequency (RF)-sputtering technique in different argon (Ar) and acetylene (C_2H_2) plasmas. The bandgap of the films can be tuned from 1.41 to 1.28 eV, which correlates with the sp^2 content, which increases from 56.3 to 63.7 %, respectively. The different ratios of sp^2/sp^3 lead to different bandgaps of the DLC films. Plasmonic nanoparticles of silver (Ag) were also embedded in the DLC matrix by reactive magnetron sputtering to study the enhancement of light absorption in DLC films. The absorption coefficient significantly increased when the DLC films were incorporated with 10 at.% of silver nanoparticles. Raman and X-ray photoelectron spectroscopy (XPS) studies were utilized to determine the bonding nature and sp^2/sp^3 ratios of DLC–Ag films.

Introduction

Solar cell market is mostly dominated by crystalline silicon solar cells, but its manufacturing cost is still high for mass consumption. In the search for alternative materials, carbon is highly attractive as it is expected to have properties similar to silicon together with high microstructural stability. Carbon exists in various stable forms like amorphous films, graphene, semiconducting fullerenes, and carbon nanotubes (CNTs) [1], which show many interesting optoelectronic, physical, and chemical properties. Amorphous carbon containing a mixture of $sp^3(\sigma)$- and $sp^2(\pi)$-hybridized bonds is known as diamond-like carbon (DLC) wherein the relative amounts of sp^3- and sp^2-bonded carbon determine the DLC film properties. For example, DLC films can be used as an absorber layer in thin-film solar cells due to its p-type conductivity [1–5].

The optical bandgap of DLC films can be tuned by changing the preparation conditions. Indeed, variations of the deposition environment can modulate the proportion between sp^3 and sp^2 bonds, determining the bandgap of the DCL film. The bandgap of the films can be tailored to match the solar spectrum [6, 7] for photovoltaic (PV) application. Consequently, multilayer DLC films with graded bandgap could absorb almost the whole solar spectrum. In particular, an absorber could be engineered with several DLC films with graded bandgap, thus greatly enhancing the photon

Address correspondence to E-mail: jadavpurphys.barun@gmail.com

DOI 10.1007/s10853-016-0324-7

absorption and efficiency of the solar cell. Light absorption in the active layer of the solar cell can also be increased by light-trapping method such as surface texturing [8], diffraction gratings [9], or resonant plasmonic structures [10–12]. Light trapping by metal nanoparticles from the first group B (Ag, Cu, and Au) having surface plasmon resonances is an attractive strategy to confine the light within the active layer of the solar cell by increasing the photon absorption and hence the efficiency of the solar cell [13–16]. Silver-doped DLC shows the surface plasmon resonance peak when the atomic percentage of silver is more than 1–2 % [17]. Ag-doped DLC films have diverse applications in solar energy [18], electronic devices [19], and optical applications [20]. Thus, incorporation of plasmonic nanoparticles in DLC films could represent an advantage in carbon-based PV only if the absorber layer has a relatively low absorption coefficient.

Different synthesis techniques like physical vapor deposition (PVD), chemical vapor deposition (CVD), thermionic vacuum arc, precipitation, and electrodeposition have been used to incorporate silver in the DLC matrix. Silver incorporation in the DLC matrix by sputtering and related surface plasmon resonance effect was reported by Paul et al. [21]. Wang et al. [22], Lungu et al. [23], Ahmed et al. [24], and Zhang et al. [25] have reported the effect of silver incorporation in DLC films for tribological applications. Nevertheless, only Zhang et al. [6] and Tinchev et al. [7] have reported the DLC film with graded bandgap for PV applications, using additional bias voltage in plasma-enhanced chemical vapor deposition (PECVD) technique.

In this communication, we present our studies on pure DLC and DLC-Ag films with graded bandgap obtained at different C_2H_2 percentages in the $Ar + C_2H_2$ plasma deposited by RF magnetron-sputtering technique. To the best of our knowledge, the changes in the optical properties of DLC films with the variations of sp^2/sp^3 ratio in sputtered films using $Ar + C_2H_2$ plasma with different C_2H_2 percentages and the increment of optical absorption in the DLC films due to surface plasmon resonance have not been reported yet for PV applications.

Experimental details

Pure DLC and silver-doped DLC films were deposited by magnetron sputtering with RF (13.56 MHz) plasma. Two sets of films were prepared. First, pure DLC films were deposited onto glass and Si (100) substrates at room temperature from a graphite target (50.8 mm diameter, 99.999 % purity, Kurt Lesker) using a mixture of acetylene and argon gases, with three different volume percentages of acetylene (20, 30, and 40 %). Second, for the silver-doped DLC film, we have used a silver target (50.8-mm diameter, 99.999 % purity, Kurt Lesker) and performed the sputtering in the same (vol%) acetylene + argon plasma. In every deposition, the RF power and substrate-to-target distance were set to 100 W and 70 mm, respectively. The whole sputtering chamber was first evacuated to a base pressure of 2.6×10^{-4} Pa before deposition, while the working pressure during the deposition was set to 1.5 Pa. The time of deposition for all the films was 60 min. Pure DLC films and Ag-doped DLC films were named as S1, S2, S3, and S1-Ag, S2-Ag, S3-Ag respectively.

The deposition technique here employed is a magnetron-sputtering/plasma CVD-composite method [26]. Sputtering from a vapor source made of solid graphite target with Ar plasma can also form a DLC film but at a very low film deposition rate due to the low carbon sputter yield, in a pure Physical Vapor Deposition (PVD) process. The deposition rate is significantly increased under a hydrocarbon gas flow (like acetylene, for example) into the sputtering chamber. The Argon plasma reacts with the C_2H_2 molecules to form a DLC film with hydrogen from the cracking products in a plasma Chemical Vapor Deposition (CVD) method. Thus, in the first set of samples (S1, S2, and S3), the graphite target has a negligible role because it only acts as an additional source of carbon atoms, which allows to grow an initial film on the substrate surface. To confirm this, we have prepared a DLC film from a graphite target and only with Ar plasma. This film had a thickness of about 15 nm measured by AFM, which is very thin compared with the DLC films of both sets of samples (In Supplementary Material, we have given more support to this affirmation). For the second set of samples (S1-Ag, S2-Ag, and S3-Ag), Ag-doped DLC, the films are totally produced from the acetylene cracked molecules in a reactive sputtering process on the silver target.

Microstructural characterizations were carried out by field-emission scanning electron microscopy (FESEM, FEI Inspect F50), transmission electron microscopy (TEM, FEI Tecnai F20 G^2), and X-ray Diffraction (XRD, Bruker D8 Advance with Cu Kα

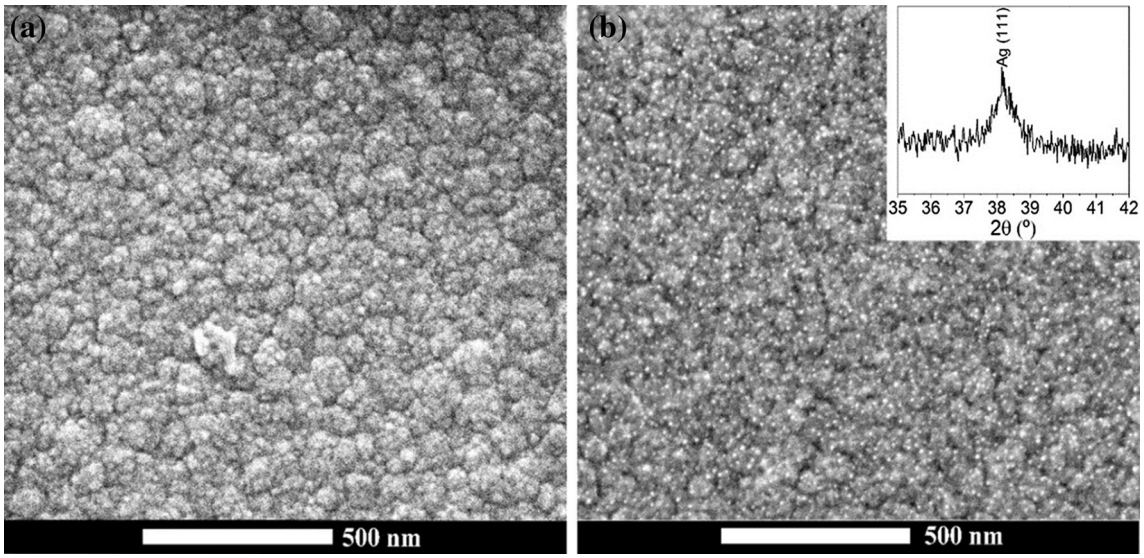

Figure 1 FESEM images of **a** pure DLC films (S2) and **b** Ag-doped DLC films (S2-Ag). *Inset* of **b** shows the XRD pattern of the film (S2-Ag).

radiation). Samples for TEM were prepared by scraping the deposited films and placing them onto a holey carbon-supported film on a copper grid. The I_D/I_G ratio and sp^2/sp^3 contents in the films were determined by Raman spectroscopy (LabRam 010 Spectrometer, $\lambda = 633$ nm) and X-ray photoemission (XPS, Physical Electronic model 1257) spectroscopy, respectively. In XPS, Al Kα line was used as the X-ray source at 1486.74 eV, while the anode was operated at 15 kV and the source power level was set to 400 W. Compositional information was obtained using an energy dispersive X-ray (EDS) detector ($EDAX^{TSL}$ analyzer). Optical studies were performed by measuring transmittance and absorbance in the wavelength region, $\lambda = 200$–900 nm, using a spectrophotometer (Perkin Elmer Lambda-11) at room temperature. The spectra were recorded with a resolution of $\lambda \sim 0.5$ nm along with a photometric accuracy of $\pm$ 0.5 % for transmittance measurements.

Results and discussion

Microstructural characterization

Figure 1 displays two representative FESEM images of pure DLC (S2) and Ag-doped DLC films (S2-Ag). It can be seen that both films have a granulated morphology covering the whole silicon surface. S2 sample exhibited grains of roughly 40 nm (Fig. 1a). All other pure DLC samples showed similar morphology despite the acetylene concentration in the plasma during preparation. Figure 1(b) depicts a FESEM image of the sample S2-Ag which shows nanoparticles of nearly 11 nm on the surface of the film. EDS measurements confirmed that the nanoparticles correspond to silver nanoparticles with a concentration of 10 at.%. Silver concentration of samples S1-Ag and S3-Ag were also measured using EDS, and the results are presented in Table 1.

Table 1 Values of different parameters of DLC and DLC-Ag films prepared by RF-sputtering technique

Film	C_2H_2 (%) in the plasma gases	Ag concentration (at.%)	Sp^2 (%)	Sp^3 (%)	I_D/I_G	E_g (eV)	Urbach energy (meV)
S1	20	–	56.3	43.7	1.12	1.41	–
S2	30	–	59.6	40.4	1.21	1.36	–
S3	40	–	63.7	36.3	1.34	1.28	–
S1-Ag	20	6	61.7	38.3	1.22	1.32	560
S2-Ag	30	10	66.6	33.4	1.33	1.20	688
S3-Ag	40	4	68.5	31.5	1.36	1.11	523

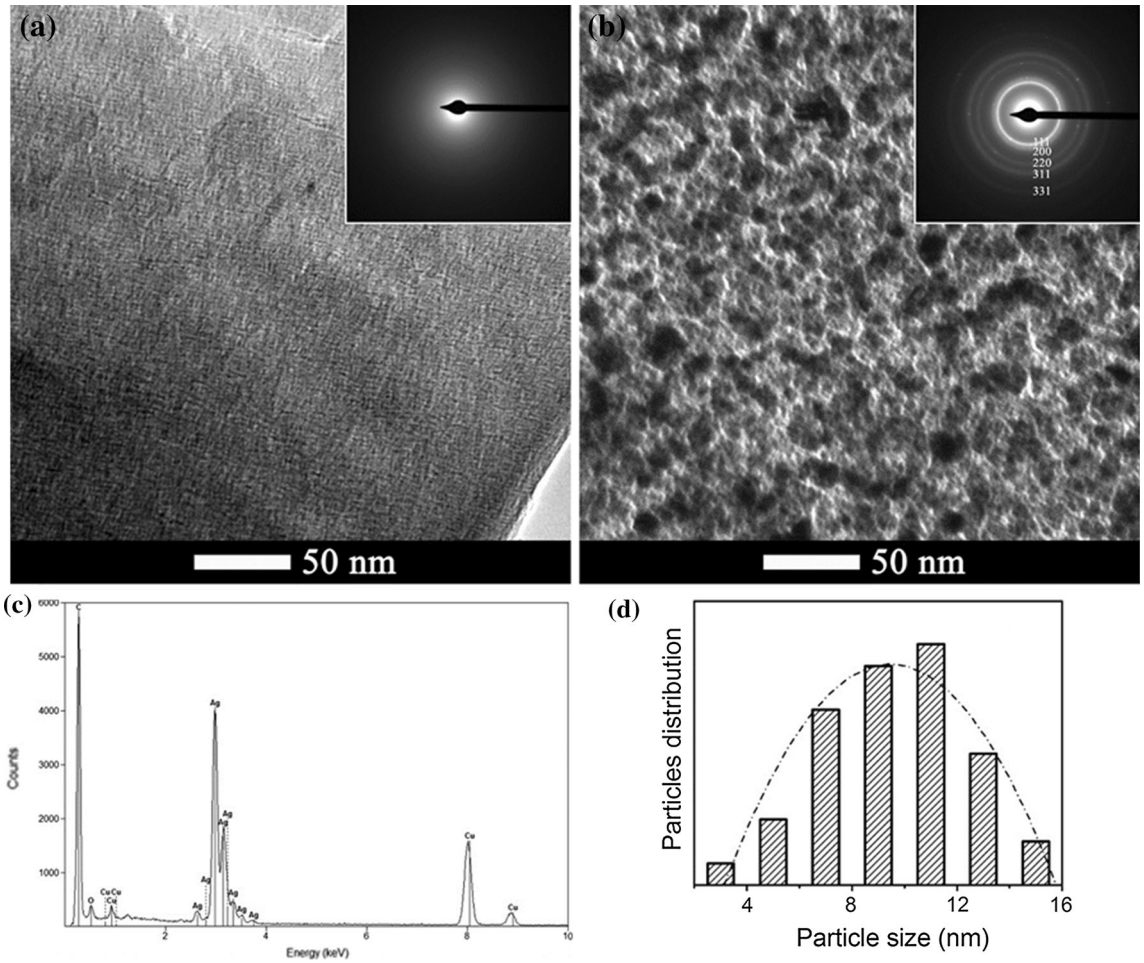

Figure 2 TEM images of **a** pure DLC films (S2) and **b** silver-doped DLC films (S2-Ag). *Inset* shows the corresponding SAED pattern, **c** EDS spectrum of the film S2-Ag (Cu signal comes from the copper grid used for TEM) and **d** particle size distribution of the corresponding film (S2-Ag).

XRD analysis of all the films under study revealed that the DLC films were deposited with an amorphous microstructure (images not shown). However, XRD pattern of Ag-doped DLC films exhibited the characteristic peak of crystalline silver nanoparticles. The inset of Fig. 1(b) shows the XRD pattern of S2-Ag films where the (111) reflection plane of Ag at $2\theta \sim 38.4^{\circ}$ is observed. Similar results were found by Baba et al. [27] in their silver-incorporated DLC films. The crystallite size was estimated using Scherrer relation which corresponds to a size of about 8 nm.

Figure 2(a, b) shows the TEM images of S2 (pure DLC) and S2-Ag samples, respectively. TEM characterization of pure DLC films confirmed the amorphous structure as shown in Fig. 2(a). The inset of this figure shows the characteristic selected area electron diffraction pattern (SAED) of amorphous materials. On the other hand, TEM observations of Ag-doped DLC films showed the presence of nanoparticles as black spots (see Fig. 2b), which were recognized as Ag nanoparticles by EDS, as shown in the spectrum of the film S2-Ag depicted in Fig. 2(c). In addition, the SAED pattern (inset of Fig. 2b) demonstrated the polycrystalline nature of these silver nanoparticles. Figure 2(d) represents the histogram of the nanoparticle size distribution of S2-Ag film. The diameter of the nanoparticles ranges between 3 and 16 nm, while the average diameter is 11 nm. Due to the addition of high atomic percentage of silver (10 at.%), some large agglomerated particles were observed in the film (S2-Ag). A similar result was observed by Yaremchuk et al. [28] in their silver-doped DLC films.

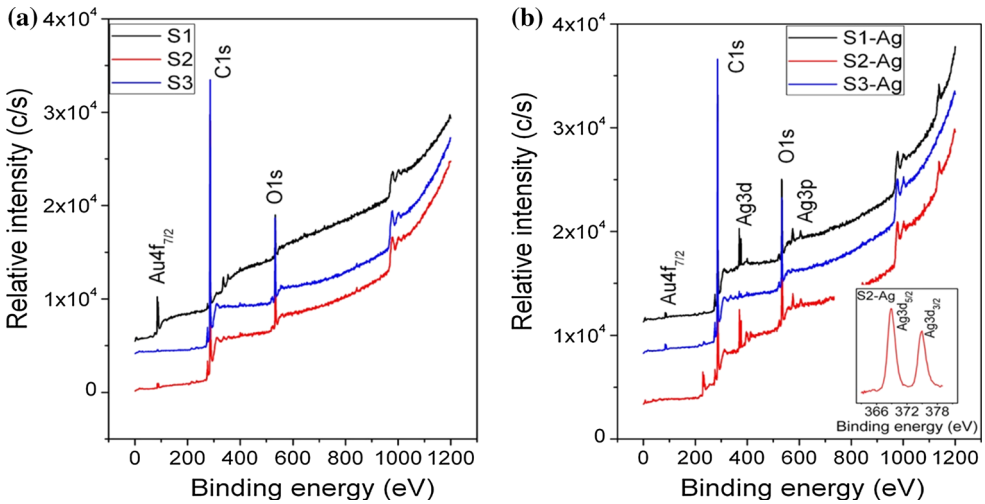

Figure 3 General survey of XPS spectra of three representative DLC films: **a** without silver and **b** with silver. *Inset* of **b** represents the core level spectra of $Ag3d_{3/2}$ and $Ag3d_{5/2}$ for the films S2-Ag.

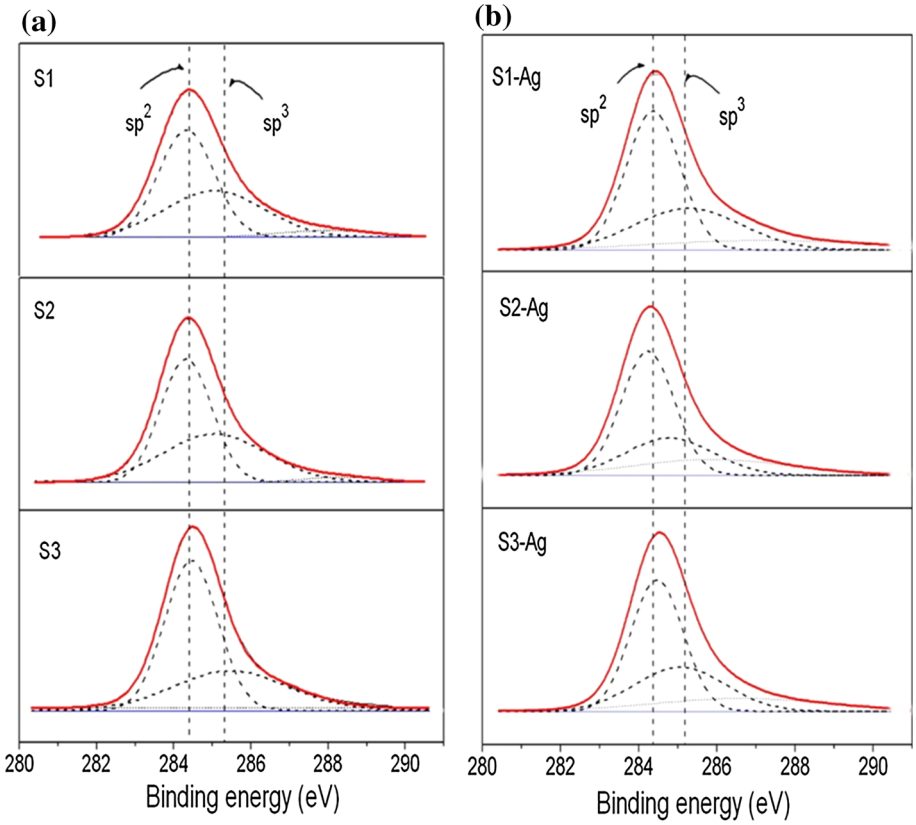

Figure 4 C1 s peak fitting of **a** pure DLC films and **b** Ag-incorporated DLC films.

XPS characterization

DLC films are the admixture of sp^2- and sp^3-bonded carbon. Thus, to determine the hybridization of carbon on the surface of the films, XPS analysis was performed. The characteristic binding energies of pure graphite and diamond are 284.2 eV (sp^2) and 286 eV (sp^3), respectively [29]. The peak positions of all the DLC films were located in between diamond (286 eV) and graphite (284.2 eV). Using Multipak software, the peaks were fitted, and the amounts of sp^2 and sp^3 % were calculated based on the fitting area.

Figure 3(a) displays the general survey of XPS spectra of three pure DLC films (S1, S2, and S3 samples). These spectra only have the peaks of C1 s

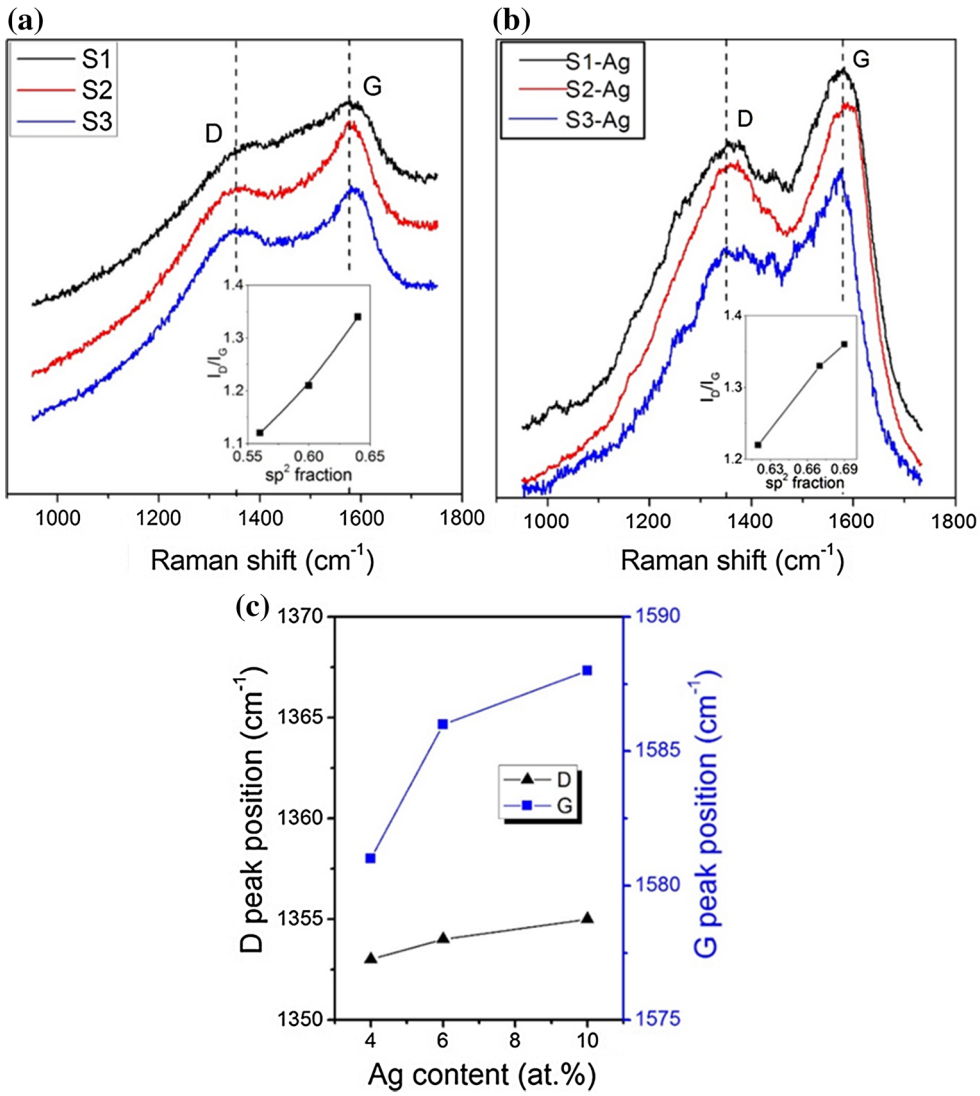

Figure 5 Raman spectra of three representative DLC films: **a** without silver and **b** with silver. *Inset* shows the variation of I_D/I_G ratio with sp^2 fraction of the corresponding films, **c** variations of D-peak and G-peak positions with silver content in the DLC films.

(~284 eV) and O1 s (~532 eV). The Au4f (~84 eV) was used as a reference peak. The O1 s peak at ~532 eV was attributed to the surface with air exposure [30]. The high-resolution C1 s peak (see Fig. 4a) was fitted with two Gaussian curves, and the percentages of sp^2 and sp^3 were calculated and are listed in Table 1. As the area of the each peak is related to the corresponding phase, we have considered the area of the sp^2 peak divided by the area of the sum of the sp^2 and sp^3 peaks for determining the sp^2 percentage in the films [29]. The sp^2 contents in the three pure DLC films were 56.3, 59.6, and 63.7 % for the samples S1, S2, and S3, respectively. This means that as the films are deposited with the increasing C_2H_2 percentages, the sp^2 content increases. Similar results were observed by Paul et al. [31] in their DLC films with different sp^2/sp^3 ratios.

Figure 3(b) shows the general survey of XPS spectra of three representative Ag-doped DLC films, in which C1 s, O1 s, Ag3d, and Ag3p can be identified. The high-resolution C1 s spectra of these films are displayed in Fig. 4(b). Analogous to pure DLC films, after fitting, it was also found that the sp^2 percentage increases from 61.7 to 68.5 % for the samples S1-Ag to S3-Ag (Table 1). The comparison between both sets of samples deposited with the same acetylene percentage during deposition indicates that the $sp^2/(sp^2 + sp^3)$ ratio overall increases with the addition of silver nanoparticles, which means that the films become more graphitic when doped with Ag nanoparticles [32]. Inset of Fig. 3(b) represents the core level XPS spectra of silver signal which corresponds to $Ag3d_{3/2}$ (~374.2 eV) and $Ag3d_{5/2}$ (~368.2 eV) for S2-Ag films. The Ag3d peaks for all

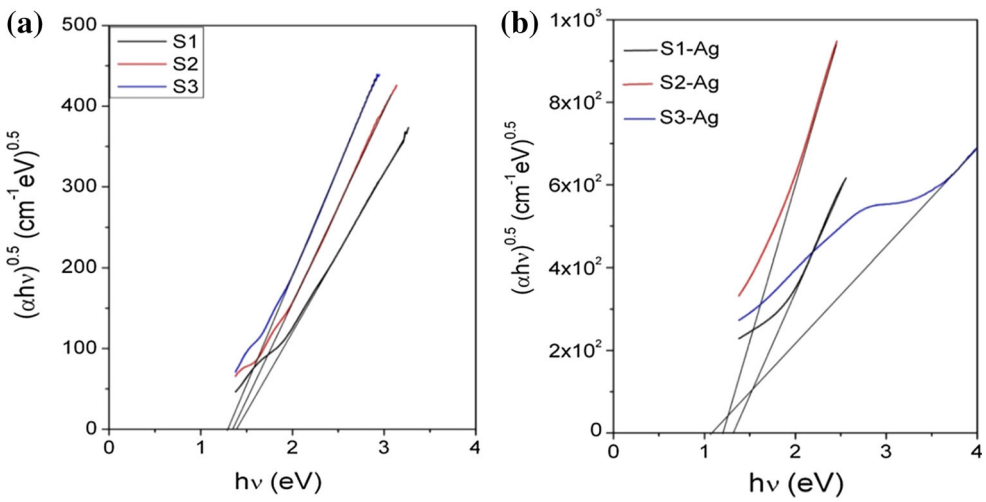

Figure 6 **a** Plots of $(\alpha h\nu)^{0.5}$ versus hν for three representative DLC films (S1, S2, and S3) deposited at glass substrate with three different C_2H_2 percentages in the Ar + C_2H_2 plasma, **b** the same plot of $(\alpha h\nu)^{0.5}$ versus hν but for the silver-doped DLC films (S1-Ag, S2-Ag, and S3-Ag).

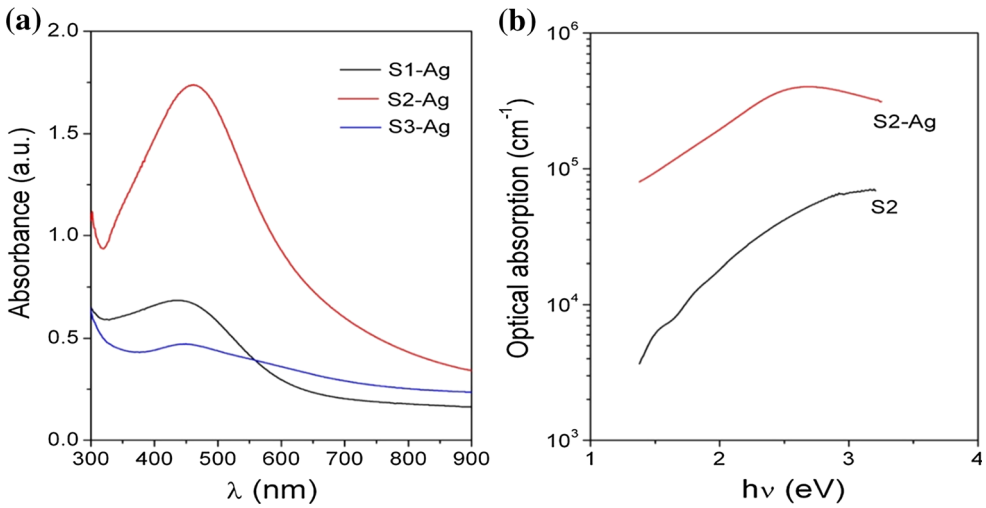

Figure 7 **a** Optical absorption spectra showing the surface plasmon resonance peak for the silver-incorporated DLC films (S1-Ag, S2-Ag, and S3-Ag) and **b** comparison of optical absorption coefficient between pure DLC (S2) and silver-doped DLC films (S2-Ag).

other films (S1-Ag and S3-Ag) were similar in nature as S2-Ag.

Raman characterization

Raman spectroscopy was performed in order to measure the disorder in the carbon films. Figure 5(a, b) shows the Raman spectra of pure DLC films (S1, S2, and S3) and Ag-doped DLC films (S1-Ag, S2-Ag, and S3-Ag), respectively. Typical Raman peaks of carbon were located at 1353 cm^{-1} (D-peak disorder) and 1588 cm^{-1} (G-graphite peak). It was observed that as the C_2H_2 content increases in the Ar plasma during the films deposition, the D peak becomes wider and the G peak becomes more intense. The spectra were fitted using two Gaussian curves, and the I_D/I_G ratios were calculated taking the intensity ratios of D and G peaks [33], which are summarized in Table 1. The variations of I_D/I_G with sp^2 content for the films without and with silver are plotted in the insets of Fig. 5(a, b), respectively. It can be seen that the I_D/I_G ratio increases with the increasing sp^2 content for both sets of samples.

The shifts of D- and G-peak positions with silver content in the doped DLC films are shown in Fig. 5(c). It may be noted here that there was no significant change in the D-peak position, while a significant shifting of the G-peak position to a higher wavenumber was observed with the increasing amount of silver in the DLC films, indicating an increase in graphite-like structure [34]. The G-peak position was shifted from 1581 cm^{-1} in sample S3-Ag to 1588 cm^{-1} in sample S2-Ag, which could be attributed to the confinement of electrons in short chains. Thus, I_D/I_G would be a measure of the size of sp^2 phase organized in rings [35]. I_D/I_G value has increased from 1.22 to 1.36

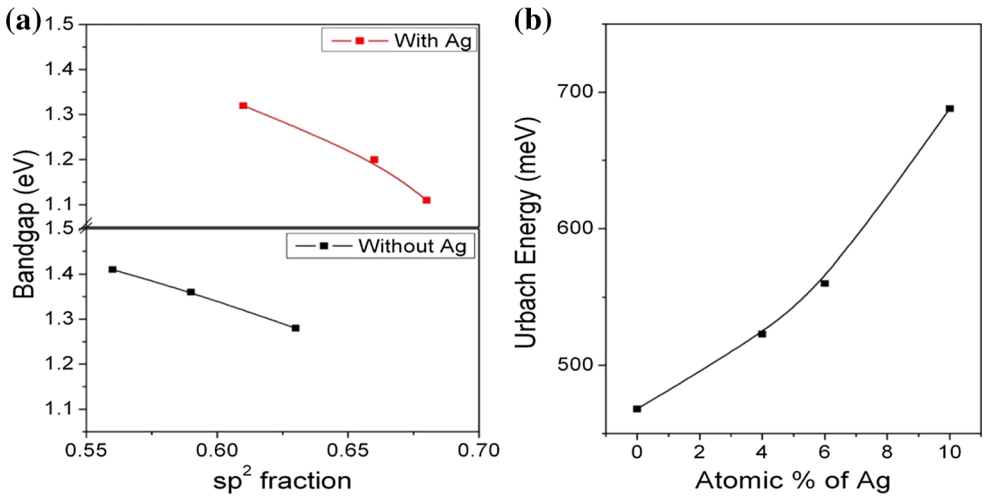

Figure 8 **a** Bandgap values with sp^2 % for the DLC films with and without silver, **b** Variation of Urbach energy (meV) with at.% of Ag in the DLC films.

as the Ag concentration increases from 4 to 10 at.% in the DLC films indicating the presence of more sp^2-bonded carbon in the films. These results are well in agreement with the XPS results.

Optical studies

Transmittance and absorbance spectra of all DLC films under study were recorded in the wavelength range between 200 and 900 nm, and from the transmission spectra, the optical bandgap was calculated. In an amorphous material like DLC, the relation between the absorption coefficients (α) and incident photon energy (hν) can be written as [31]

$$(\alpha h\nu) = A(h\nu - E_g)^2, \quad (1)$$

where A is a constant, and E_g is the optical bandgap of the material. Extrapolating the linear portion of the $(\alpha h\nu)^{0.5}$ versus hν plot to the hν axis at $\alpha = 0$, the optical bandgap can be calculated from the intercept, as shown in Fig. 6(a). Bandgap values for pure DLC films (S1, S2, and S3) decrease from 1.41 to 1.28 eV (Table 1) with the increasing C_2H_2 percentage in the plasma. This decrease of E_g is attributed to the passivation of dangling bonds present in the DLC films by hydrogen from the plasma CVD-composite process during the sputtering deposition [36]. As a result, more localized states in the bandgap region lead the band tailing, and hence the bandgap decreases with the increasing C_2H_2 percentages [31]. From the E_g calculations, a graded bandgap is observed in the DLC films, which could be an effective absorber layer for DLC multilayer (n-DLC/multilayer i-DLC/p-DLC) thin-film solar cell [6].

The determination of the optical bandgap of the Ag-doped DLC films is shown in Fig. 6(b), where E_g

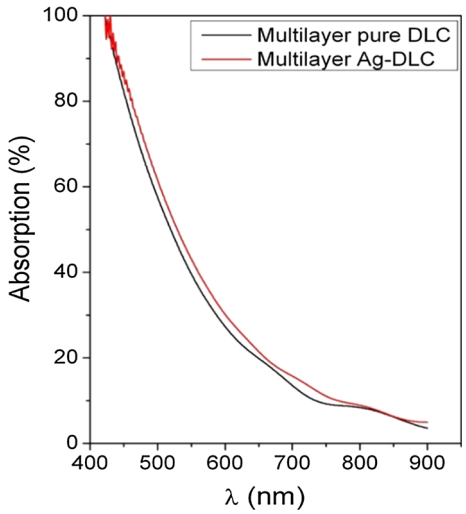

Figure 9 Comparison of optical absorptions between pure DLC multilayer thin film and Ag-doped DLC multilayer film.

values also decreased with the increasing C_2H_2 percentage in the plasma and with the increasing sp^2 content in the films, as determined by XPS. The E_g values varied from 1.32 to 1.11 eV. The highest bandgap was obtained with the lowest sp^2 %.

Generally, when the films are embedded with nanocrystalline metal particles separated from each other by a certain distance, the properties of these films are different from those of the bulk. The interaction of these nanoparticles with the electromagnetic field would result in a coherent oscillation of the conduction electrons called the surface plasmon resonance (SPR) [35]. The surface plasmon resonance peaks for the silver-doped DLC films are shown in Fig. 7(a). All the doped films (S1-Ag, S2-Ag, and S3-Ag) have a surface plasmon resonance peak around

460 nm. The nature and position of the plasmonic peak depend on the size, shape, and the dielectric medium (here DLC) embedding the metal nanoparticles. The films prepared with 20 and 40 % (v/v) of C_2H_2 showed a relatively lower intense and broad SPR peak rather than the films prepared with 30 vol% of acetylene would do. From EDS analysis, the measured silver atomic concentration for three DLC-Ag films was 6, 10, and 4 % for the samples S1-Ag, S2-Ag, and S3-Ag, respectively. Therefore, a maximum intense SPR peak was observed when the DLC films have 10 at.% of silver nanoparticles (S2-Ag). A slight red shift of the plasmonic peak was also observed for the film S2-Ag. When the density of silver nanoparticles increases in the DLC matrix, the distance between particles decreases which helps to increase the coalescence in the films. As a result, the red shift of the plasmonic peak could be observed [35]. The intensity of the SPR peak also increased with the increase of Ag atomic concentration in DLC films. In Supplementary Material, we present the plot with the absorbance curves of both sets of samples, and the sample prepared only with Ar plasma shows a very low absorbance for this last film, which also demonstrates its very low thickness.

The comparison of the optical absorption coefficients of S2 and S2-Ag films is shown in Fig. 7(b). The optical absorption coefficient has increased by one order of magnitude when the DLC film was doped with 10 at.% of Ag nanoparticles. It is clearly seen that the absorption is higher in the lower wavelength region, and hence it matches very well with the solar spectrum [7]. We have measured the thickness of the films by AFM line profile analysis. Both films (S2 and S2-Ag) have nearly the same thickness of about 600 nm. Therefore, this difference in the absorption coefficient is due to the surface plasmon effect in DLC films. A DLC multilayer film with graded bandgap and the incorporation of silver nanoparticles inside the matrix would give enhanced optical absorption rather than a pure DLC multilayer film with graded bandgap would do. These results suggest that the graded bandgap DLC multilayer films with plasmonic nanoparticles can be used for enhancing the absorption in carbon-based solar cells.

The variable, E_g, of the sp^2 sites depends on the configuration of π states in the valance band and π* states in the conduction band. The increasing bandgap with decreasing sp^2 content is attributed to the decrease in the width of the π and π* bands [3]. The variations of the bandgap with sp^2 % for the DLC films with and without silver are shown in Fig. 8(a). It was observed that with the addition of silver nanoparticles, the bandgap of the films with the same vol% of C_2H_2 was slightly less than that of the films without silver.

In an amorphous material like diamond-like carbon, the valence band and conduction band do not have sharp cutoffs but they have tails of localized states in the lower energy region. Because of this, when the Tauc plot is made for the determination of the optical bandgap, it does not form a straight line in the whole energy range. In such cases, Urbach energy is a measurement of the inhomogeneous disorder of amorphous carbon films [37]. Urbach band tail is expressed by [32]:

$$\ln\alpha = \ln\alpha_0 - h\nu/E_u, \quad (2)$$

where α is the absorption coefficient, hν is the incident photon energy, α_0 is a constant, and E_u is the Urbach energy. Basically, Urbach band tails are responsible for all the possible defects in semiconductors like DLC [32]. E_u values for the three different Ag-doped DLC films were estimated from the slopes of the linear plot of lnα versus hν and their values are plotted as a variation of the atomic percentage of silver in Fig. 8(b). It may be noted that the defect density in the Ag-incorporated DLC films increases with the silver concentration (Table 1).

Finally, with the aim of preparing a p–i–n structure, we have fabricated a pure DLC multilayer thin film using three sublayers with optimum bandgap of 1.41, 1.36, and 1.28 eV. The tunable bandgap was obtained by varying the acetylene percentage in the RF plasma during the deposition of each sublayer. Another DLC multilayer thin film with optimal bandgap was fabricated in a similar way but with the addition of silver nanoparticles in the second layer. The optical absorption spectra of these films is shown in Fig. 9. The optical absorption of the multilayer thin film with silver nanoparticles is higher than the absorption of pure DLC multilayer thin film. Moreover, the absorption is higher in the lower wavelength region, and it decreases with the increasing λ, which matches very well with the solar spectrum [38]. The p–i–n structure is the most appropriate for high electric-resistive materials like DLC solar cell. The graded optical bandgap would have an additional advantage, but before going for the fabrication of the solar cell, it is necessary to optimize the

thickness of each layer to obtain the higher electric field, which will be beneficial for rearranging the space charge and collecting the photogenerated carriers [7]. We have already started this work, and this will be a topic for a future study.

Conclusions

We have successfully deposited DLC films with tunable optical bandgap (E_g) on glass and Si (100) substrates by RF-sputtering combined technique from a graphite target in different argon (Ar) and acetylene (C_2H_2) plasma mixtures. The bandgap of the films has decreased from 1.41 eV to 1.28 eV with an increase in sp^2 % from 56.3 to 63.7 % in these films. The different ratios of sp^2/sp^3 in the films result in different bandgaps which would cover the solar spectrum for PV application. We have also incorporated plasmonic nanoparticles of silver (Ag) in the DLC matrix to study the enhancement of light absorption. The absorption coefficient has increased by at least one order of magnitude when the DLC films were doped with 10 at.% of silver nanoparticles. The polycrystalline nature of Ag nanoparticles was confirmed by XRD and electron diffraction from TEM analysis. A combination of pure and silver-doped DLC films was used to prepare a multilayer structure with graded bandgap which showed higher optical absorption than a pure DLC multilayer structure. Thus, DLC multilayer thin films with plasmonic nanoparticles can be used for enhancing the absorption in carbon-based solar cells.

Acknowledgements

The authors would like to thank π-NANO Anillo Project ACT-1117, Fondecyt Project N° 1150652, and Postdoctoral Fondecyt Project N° 3140565. BG wishes to thank Prof. Víctor Fuenzalida, the Department of Physics, Universidad de Chile, and Roberto Villarroel, a PhD student from the same University for their kind support.

Electronic supplementary material: The online version of this article (doi:10.1007/s10853-016-0324-7) contains supplementary material, which is available to authorized users.

References

[1] Zhu H, Wei J, Wang K, Wu D (2009) Applications of carbon materials in photovoltaic solar cells. Sol Energy Mater Sol Cells 93:1461–1470

[2] Ghosh B, Ghosh D, Ghosh A, Hussain S, Bhar R, Pal AK (2014) Electrodeposited diamond-like carbon (DLC) films on n-Si(100) substrates for photovoltaic application. Mater Sci Semicond Process 25:130–136

[3] Kalaga K, Umeno M, Nukaya Y, Soga T, Jimbo T (2000) Photovoltaic and spectral photoresponse characteristics of nC/pC solar cell on a p-silicon substrate. Appl Phys Lett 77(10):1472–1474

[4] Ma ZQ, Liu BX (2001) Boron-doped diamond-like amorphous carbon as photovoltaic films in solar cell. Sol Energy Mater Sol Cells 69(4):339–344

[5] D. Ghosh, B. Ghosh, Anindita Ghosh, S. Hussain, R. Bhar, A.K. Pal (2013) Carbon based PV: n-Si(100)/DLC structure for photovoltaic application. ISRN-Renew Energy, 851876. doi: 10.1155/2013/851876

[6] M. Zhang, X. Cheng, C. Chen (2008) Research of diamond-like carbon (DLC) films: promising candidate for absorber layer of Solar Cells. Sixth International Conference on Thin Film Physics and Applications, Proceedings of SPIE, 6984:69843E. doi:10.1117/12.792179

[7] Tinchev SS, Nikolova PI, Dyulgerska JT, Danev G, Babeva Tz (2005) a-C: h absorber layer for solar cells matched to solar spectrum. Sol Energy Mater Sol Cells 86(3):421–426

[8] Despeisse M, Battaglia C, Boccard M, Bugnon G, Charriere M, Cuony P, Hanni S, Lofgren L, Meillaud F, Parascandolo G, Soderstrom T, Ballif C (2011) Optimization of thin film silicon solar cells on highly textured substrates. Phys status solidi (a) 208:1863–1868

[9] Mellor A, Tobías I, Martí A, Mendes MJ, Luque A (2011) Upper limits to absorption enhancement in thick solar cells using diffraction gratings. Prog Photovolt Res Appl 19:676–687

[10] Atwater HA, Polman A (2010) Plasmonics for improved photovoltaic devices. Nat Mater 9:205–213

[11] Hairen T, Santbergen R, Guangtao Y, Smets AHM, Zeman M (2013) Combined Optical and Electrical Design of Plasmonic Back Reflector for High-Efficiency Thin-Film Silicon Solar Cells. IEEE J Photovolt 3:53–58

[12] Morawiec S, Mendes MJ, Mirabella S, Simone F, Priolo F, Crupi I (2013) Self-assembled silver nanoparticles for plasmon-enhanced solar cell back reflectors: correlation between structural and optical properties. Nanotechnology 24:265601–265611

[13] Pillai S, Catchpole KR, Trupke T, Green MA (2007) Surface plasmon enhanced silicon solar cells. J Appl Phys 101:093105–093108

[14] Polman A (2008) Plasmonics applied. Science 322:868–869
[15] Catchpole KR, Polman A (2008) Plasmonic solar cells. Opt Express 16:21793–21800
[16] Ghosh B, Ghosh D, Hussain S, Chakraborty BR, Sehgal G, Bhar R, Pal AK (2014) Inclusion of nano-Ag plasmonic layer enhancing the performance of p-Si/CdS solar cells. Phys Status Solidi A 211(4):890–900
[17] Měskinisa S, Ciegisa A, Vasiliauskas A, Tamulevi̇cieńe A, Slapikas K, Jǔsḱenas R, Niaura G, Tamulevi̇cius S (2014) Plasmonic properties of silver nanoparticles embedded in diamond like carbon films: influence of structure and composition. Appl Surf Sci 317:1041–1046
[18] Tritsaris G, Mathioudakis C, Kelires P, Kaxiras E (2012) Optical and elastic properties of diamond-like carbon with metallic inclusions: a theoretical study. J Appl Phys 112:103503–103506
[19] Narayan R, Scholvin D (2005) Nanostructured carbon-metal composite films. J Vac Sci Technol B 23:1041–1046
[20] Yaremchuk I, Tamulevičienė A, Tamulevičius T, Šlapikas K, Balevičius Z, Tamulevičius S (2014) Modeling of the plasmonic properties of DLC-Ag nanocomposite films. Phys Status Solidi (a) 211:329–335
[21] Paul R, Gayen RN, Hussain S, Khanna V, Bhar R, Pal AK (2009) Synthesis and characterization of composite films of silver nanoparticles embedded in DLC matrix prepared by plasma CVD technique. Euro Phys J Appl Phys 47:10502–10513
[22] Wang C, Yu X, Hua M (2009) Microstructure and mechanical properties of Ag-containing diamond-like carbon films in mid-frequency dual-magnetron sputtering. Appl Surf Sci 256:1431–1435
[23] Lungu CP (2005) Nanostructure influence on DLC-Ag tribological coatings. Surf Coat Technol 200:198–202
[24] Ahmed SF, Moon MW, Lee KR (2008) Enhancement of electron field emission property with silver incorporation into diamondlike carbon matrix. Appl Phys Lett 92:193502–193504
[25] Zhang HS, Endrino JL, Anders A (2008) Comparative surface and nano-tribological characteristics of nanocomposite diamond-like carbon thin films doped by silver. Appl Surf Sci 255:2551–2556
[26] Moriguchi H, Ohara H, Tsujioka M (2016) History and Application of Diamond-Like Carbon Manufacturing Processes. Sei Tech Rev 82:52–58
[27] K. Baba, R. Hatada, S. Flege, W. Ensinger (2012) Preparation and properties of Ag-containing diamond-like carbon films by magnetron plasma source ion implantation, Adv. Mater. Sci. Eng. 2012(2012):536853. doi: 10.1155/2012/536853
[28] Yaremchuk I, Meškinis Š, Fitio V, Bobitski Y, Šlapikas K, Čiegis A, Balevičius Z, Selskis A, Tamulevičius S (2015) Spectroellipsometric characterization and modeling of plasmonic diamond-like carbon nanocomposite films with embedded Ag nanoparticles. Nanoscale Res Lett 10:157–163
[29] Hussain S, Ghosh D, Ghosh B, Bhar R, Pal AK (2013) Growth of carbon nanostructures on p-, i- and n-Si substrates by electrochemical route. J Phys D Appl Phys 46:355301–355308
[30] Holland L, Ojha SM (1979) The growth of carbon films with random atomic structure from ion impact damage in a hydrocarbon plasma. Thin Solid Films 58:107–116
[31] Paul R, Das SN, Dalui S, Gayen RN, Roy RK, Bhar R, Pal AK (2008) Synthesis of DLC films with different sp^2/sp^3 - ratios and their hydrophobic behaviour. J Phys D Appl Phys 41:055309–055315
[32] Ahmed SF, Moon MW, Lee KR (2009) Effect of silver doping on optical property of diamond like carbon films. Thin Solid Films 517:4035–4038
[33] Ferrari AC, Robertson J (2000) Interpretation of Raman spectra of disordered and amorphous carbon. Phys Rev B 61(20):14095–14107
[34] Robertson J (2002) Diamond-like amorphous carbon. Mater Sci Eng R 37:129–281
[35] Paul R, Hussain S, Majumder S, Varma S, Pal AK (2009) Surface plasmon characteristics of nanocrystalline gold/DLC composite films prepared by plasma CVD technique. Mater Sci Eng B 164:156–164
[36] Grill A (1999) Electrical and optical properties of diamond-like carbon. Thin Solid Films 355–356:189–193
[37] Tauc J, Grigorovic R, Vancu A (1966) Optical Properties and Electronic Structures of Amorphous Germanium. Phys Status Solidi 15:627–637
[38] Lux-Steiner MCh, Willeke G (2001) Strom von der Sonne. Phys Bl 57:47–53